

Second-harmonic generation involving valence-subband transitions in p -doped GaAs/Al_xGa_{1-x}As quantum wells

A. Bitz, M. Marsi, E. Tuncel, S. Gürtler, and J. L. Staehli

Institut de Physique Appliquée, Ecole Polytechnique Fédérale de Lausanne, CH-1015 Lausanne, Switzerland

B. J. Vartanian

Solid State Laboratory, Stanford University, Stanford, California 94305

M. J. Shaw

Department of Physics, The University of Newcastle upon Tyne, Newcastle upon Tyne NE1 7RU, United Kingdom

A. F. G. van der Meer

FOM Institute for Plasma Physics "Rijnhuizen," Nieuwegein, The Netherlands

(Received 17 March 1997)

We present second-harmonic generation experiments in p -doped asymmetrically stepped quantum wells using the emission of a free-electron laser in the wavelength interval between 13 and 18 μm . The wells are designed such that the three lowest valence-subbands are about equally spaced. We measured the angular and frequency dependence of the second-harmonic signal excited by intense laser irradiation chosen to be nearly resonant with the transitions between the three lowest valence subbands. We see evidence of the optical second-order susceptibility components $\chi_{xxz}^{(2)}$, $\chi_{zxx}^{(2)}$ and $\chi_{zxy}^{(2)}$, $\chi_{xyz}^{(2)}$ in the quantum wells and determine their enhancement with respect to $\chi_{xyz}^{(2)}$ of bulk GaAs. [S0163-1829(97)05440-4]

I. INTRODUCTION

It has been shown that the intersubband transitions in III-V semiconductor quantum wells (QW's) can strongly contribute to the nonlinear optical susceptibilities.^{1,2} Enhancements as big as three orders of magnitude in the second-order susceptibility have been observed in doubly resonant second-harmonic (SH) generation experiments.³⁻⁵ In these experiments, the samples, n -doped multiple quantum wells (MQW's), feature transition energies between the lowest and second, and between the second and third electronic subbands that are equal. The only element of the susceptibility tensor that exhibits a strong resonant enhancement in these n -doped structures is $\chi_{zzz}^{(2)}$ (z is the growth direction, perpendicular to the layer planes, as shown in Fig. 2).^{1,6} Thus, the exciting and generated electric fields have to be polarized parallel to the z axis. This is normally difficult to achieve and limits therefore the usefulness of the $\chi_{zzz}^{(2)}$ for device applications.

We know of only a few attempts to investigate optical nonlinearities using intra-valence-band transitions in p -doped structures.^{7,8} In contrast to the conduction subbands, the dispersion versus wave vector k in the layer plane is different for each valence subband, leading to a relatively low joint density of states for intersubband transitions.⁹ Therefore the enhancements which can be obtained in p -doped structures are expected to be lower. However, the presence of nondiagonal elements in the susceptibility tensor of p -doped structures, such as $\chi_{xyz}^{(2)}$, $\chi_{zxy}^{(2)}$, $\chi_{xxz}^{(2)}$, and $\chi_{zxx}^{(2)}$, provides more functionality, since the incoming fundamental and the outgoing SH waves can have various polarizations. Indeed the previous studies of p -doped structures have dem-

onstrated exactly this. These studies were based on structures with a single bound-to-bound resonant transition (between the spin split-off and heavy-hole subbands), and consequently exhibited a smaller enhancement over bulk than might be expected. The observation of the enhancement effect was limited by the quality of the available samples, reflected in the large linewidths observed experimentally. In the present study, the structures were designed to enable doubly resonant processes between heavy-hole (HH) and light-hole (LH) subbands, increasing the level of expected enhancement.

In this paper, we report SH generation experiments on p -doped asymmetrically stepped MQW's using as an exciting source the beam of a free-electron laser (FEL). We see evidence of the influence of the elements $\chi_{xyz}^{(2)}$, $\chi_{zxy}^{(2)}$, $\chi_{xxz}^{(2)}$, and $\chi_{zxx}^{(2)}$ in the SH emission of our structure. This paper is organized as follows. In Sec. II we present the design of the investigated sample. The third section gives a very brief summary of the theory and its predictions. In Sec. IV we present the experimental results including photoluminescence (PL) and the measured angular, polarization, and frequency dependence of the SH signal. The results are then discussed in Sec. V and compared to the theoretical predictions.

II. SAMPLES

The design of the sample structure was determined by the following conditions: (1) We used the GaAs/Al_xGa_{1-x}As heterostructure system because of its well-known material parameters and the well-established sample growing procedures. (2) The intersubband transition energies must be higher than the phonon energies of GaAs (35 meV), to avoid

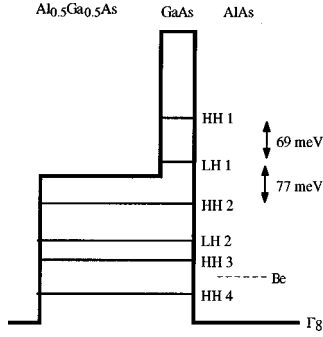


FIG. 1. Energy level scheme of the valence subbands, as calculated for a 4(GaAs)-14(Al_{0.5}Ga_{0.5}As)-12(AlAs) MQW structure (Ref. 7). The thick lines represent the potential felt by the valence-band electrons in effective-mass approximation, the thinner horizontal lines indicate the bottom of the different subbands, and the dashed horizontal line indicates the Be acceptor level in the AlAs barrier. The arrows indicate the transitions that are approximately resonant with the FEL radiation used in our SH generation experiment.

strong absorption of the exciting beam in the substrate. (3) Because the experiments were carried out in air, the fundamental and SH wavelengths were selected to be in spectral regions where the absorption by the atmospheric molecules is low. (4) For a doubly resonant experiment involving three equally spaced valence subbands, the maximum valence-band offset of about 0.5 eV that can be achieved in the GaAs/Al_xGa_{1-x}As system determines the minimum generated SH wavelength. (5) Optical transitions between subband states of the same parity (LH1-HH2) are prohibited in a symmetric quantum well.⁹ We adopted an asymmetrically stepped quantum-well structure in order to break this parity selection rule.¹ The structures satisfying all these conditions involve the HH1-LH1 and the LH1-HH2 transitions absorbing the incident fundamental beam in the wavelength range between 14 and 22 μm, and the HH2-HH1 transition emitting the SH beam.

The investigated sample was grown by molecular-beam epitaxy at a substrate temperature of 620 °C on a (001) semi-insulating GaAs wafer. The structure consists of a 500 Å-thick GaAs layer, a 4000 Å Al_{0.5}Ga_{0.5}As buffer, a 160-period 4(GaAs)-14(Al_{0.5}Ga_{0.5}As)-12(AlAs) MQW structure having a total thickness of 1.38 μm, and a 200 Å-thick GaAs capping layer. The central four monolayers of the AlAs barriers were Be doped to a concentration of $8 \times 10^{18} \text{ cm}^{-3}$; thus the nominal hole concentration in the GaAs wells should amount to $N_p = 9.2 \times 10^{11} \text{ cm}^{-2}$ per well.

III. THEORY

The band structure of the MQW's has been modeled using a semiempirical pseudopotential calculation. The optical

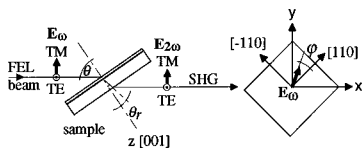


FIG. 2. Sketch of the geometry of the SH generation experiments, showing on the left the plane of the transmitted FEL beam through the sample, on the right the FEL polarization vector projected onto the plane of the sample. Note the definitions of the angles θ , θ_r , and φ , determining the orientation of the sample.

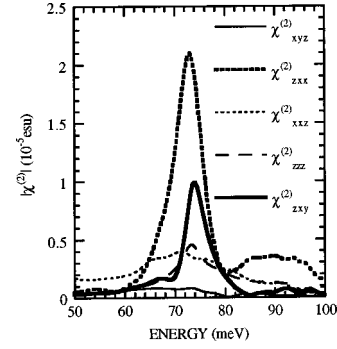


FIG. 3. The five nonzero components of the optical second-order susceptibility for a 4(GaAs)-14(Al_{0.5}Ga_{0.5}As)-12(AlAs) MQW structure with a sheet carrier concentration of $9.2 \times 10^{11} \text{ cm}^{-2}$ /well, calculated as described in Ref. 7. At resonance, i.e., at about 73 meV, the strongest components are $\chi_{zxy}^{(2)}$ and $\chi_{zxx}^{(2)}$.

susceptibilities are then obtained by applying a density-matrix theory. The theoretical details are discussed in Ref. 7. The frequency dependence of the second-order susceptibility tensor $\chi^{(2)}(-2\omega; \omega, \omega)$ has been calculated for different structures and doping concentrations, in order to permit the design of the MQW structure described above. The energy diagram plotted in Fig. 1 shows the theoretical predictions for the confined valence-band states in the investigated 4(GaAs)-14(Al_{0.5}Ga_{0.5}As)-12(AlAs) asymmetrically stepped MQW with a sheet hole density in the wells of $N_p = 9.2 \times 10^{11} \text{ cm}^{-2}$ /well. The energies for the HH1-LH1 and the LH1-HH1 transitions are predicted to be 69 meV and 77 meV, respectively, including a shift of the HH1 subband due to exchange interaction by 20 meV.⁷

For the GaAs substrate with point-group symmetry T_d the only nonvanishing independent element of the second-order susceptibility tensor $\chi^{(2)}(-2\omega; \omega, \omega)$ is $\chi_{xyz}^{(2)}$.⁶ For an asymmetrically stepped MQW structure with C_{2v} point symmetry, there are five independent nonzero elements: $\chi_{xyz}^{(2)}$, $\chi_{zxy}^{(2)}$, $\chi_{xxz}^{(2)}$, $\chi_{zxx}^{(2)}$, and $\chi_{zzz}^{(2)}$.⁷ The directions x , y , and z are defined as shown in Fig. 2. The magnitudes of these components, as calculated for the above structure, are shown in Fig. 3. The components $\chi_{zxy}^{(2)}$ and $\chi_{zxx}^{(2)}$ are predicted to be the strongest ones with a resonance at 73 meV. The $\chi_{zzz}^{(2)}$ component, which is the dominant one in structures based on conduction subband transitions,^{3,5,10} is expected to be weaker in our p -doped structures.

The second-order polarization can be expressed as¹¹

$$P_i^{(2)}(2\omega) = \sum_{j,k} \chi_{ijk}^{(2)}(-2\omega, \omega, \omega) E_j(\omega) E_k(\omega) \quad (1)$$

The component parallel to the polarization of the incident fundamental beam in the crystal can then be written as⁷

$$\begin{aligned} \frac{\mathbf{P}^{(2)}(\theta, \varphi) \cdot \mathbf{e}_\omega}{E^2(\omega)} &\propto (2\chi_{xyz}^{(2)} + \chi_{zxy}^{(2)}) \sin\theta_r \cos^2\theta_r \cos 2\varphi \\ &+ (2\chi_{xxz}^{(2)} + \chi_{zxx}^{(2)}) \sin\theta_r \cos^2\theta_r + \chi_{zzz}^{(2)} \sin^3\theta_r. \end{aligned} \quad (2)$$

The angles θ , θ_r , and φ are defined in Fig. 2. The three terms in Eq. (2) can be distinguished through their different

dependencies on the angles θ_r and φ . The coherence length l_c of a layer or structure is defined as^{5,11}

$$l_c = \frac{\pi c}{2\omega(n_{2\omega} - n_\omega)}, \quad (3)$$

where n_ω and $n_{2\omega}$ are the refractive indices at the fundamental and second-harmonic frequencies. If the thickness L_{MQW} of the MQW structure is much smaller than the coherence length, the phase mismatch of the SH signal generated in the different wells can be ignored. The SH emission intensity $I_{2\omega}$ of the whole MQW structure can therefore be taken to grow linearly with the thickness. We therefore get for a transversal magnetic (TM) wave

$$\frac{I_{2\omega}^{\text{TM/TM}}}{I_\omega^2} \propto T_{\text{TM}}^2(\theta, \omega) T_{\text{TM}}(\theta, 2\omega) A(\theta) L_{\text{MQW}} \left| \frac{\mathbf{P}^{(2)}(\theta, \varphi) \mathbf{e}_{2\omega}}{E^2(\omega)} \right|^2, \quad (4)$$

where I_ω is the intensity of the incident beam $T_{\text{TM}}(\theta, \omega)$ and $T_{\text{TM}}(\theta, 2\omega)$ are the transmission coefficients from air to GaAs for the fundamental and SH beams in TM polarization, and $A(\theta) = \cos\Theta/\cos\Theta_r$ accounts for the dependence of the refracted beam's diameter and excitation density on the sample orientation.

The SH signal of the GaAs substrate is superimposed to that of the MQW. Equation (2) applies again, with the only nonzero component $\chi_{xyz}^{(2)}$. The substrate being relatively thick, the phase mismatch of the SH wave with respect to the fundamental one has to be taken into account. This phase mismatch, at a depth d below the surface, amounts to

$$\zeta(d) = \frac{\pi}{2} \frac{d}{l_c \cos\theta_r}. \quad (5)$$

For the SH intensity generated in the substrate and integrated over the substrate thickness L_{Sub} we get¹¹

$$\begin{aligned} \frac{I_{2\omega}^{\text{TM/TM}}}{I_\omega^2} &\propto T_{\text{TM}}^2(\theta, \omega) T_{\text{TM}}(\theta, 2\omega) A(\theta) \\ &\times \left| L_{\text{SUB}} \frac{\sin\zeta}{\zeta} e^{i\zeta} 3\chi_{xyz}^{(2), \text{GaAs}} \sin\theta_r \cos^2\theta_r \cos 2\varphi \right|^2, \end{aligned} \quad (6)$$

where $\xi \equiv \xi(L_{\text{Sub}})$.

Finally, we obtain the component of the total SH intensity that is polarized in the same direction as the incident laser field (cf. Fig. 2),¹¹

$$\begin{aligned} \frac{I_{2\omega}^{\text{TM/TM}}}{I_\omega^2} &\propto T_{\text{TM}}^2(\theta, \omega) T_{\text{TM}}(\theta, 2\omega) A(\theta) \\ &\times \left(L_{\text{SUB}} \frac{\sin\zeta}{\zeta} e^{i\zeta} 3\chi_{xyz}^{(2), \text{GaAs}} + L_{\text{MQW}} \right. \\ &\times \left. (2\chi_{xyz}^{(2), \text{QW}} + \chi_{zyx}^{(2), \text{QW}}) \right) \sin\theta_r \cos^2\theta_r \cos 2\varphi \\ &+ L_{\text{MQW}} (2\chi_{xxz}^{(2), \text{QW}} + \chi_{zxx}^{(2), \text{QW}}) \sin\theta_r \cos^2\theta_r \\ &+ L_{\text{MQW}} \chi_{zzz}^{(2), \text{QW}} \sin^3\theta_r \Big|^2. \end{aligned} \quad (7a)$$

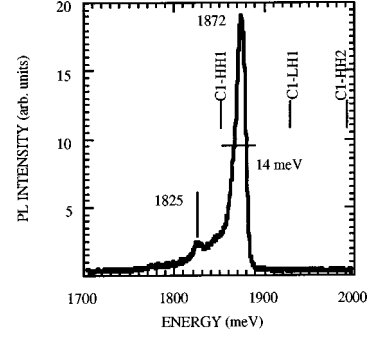


FIG. 4. Photoluminescence spectrum of the investigated MQW structure at a temperature of 2 K. The main emission line at 1872 meV is assigned to the type I transition between the lowest conduction miniband and the heavy-hole subband. The emission at 1825 meV is a phonon replica (see text). The excitation density was 4 W/cm² and the spectral resolution 2.5 meV. The labeled vertical lines indicate the calculated spectral positions of the three lowest transitions.

Equation (7a) applies to the particular case of TM polarization of the incident and SH beams (TM/TM configuration). For TE/TE configuration, it turns out that

$$\frac{I_{2\omega}^{\text{TE/TE}}}{I_\omega^2} = 0. \quad (7b)$$

For crossed polarization configurations one gets

$$\begin{aligned} \frac{I_{2\omega}^{\text{TM/TE}}}{I_\omega^2} &\propto T_{\text{TM}}^2(\theta, \omega) T_{\text{TE}}(\theta, \omega) A(\theta) \\ &\times \left(L_{\text{SUB}} \frac{\sin\zeta}{\zeta} e^{i\zeta} 2\chi_{xyz}^{(2), \text{GaAs}} \cos\theta_r \right. \\ &\left. + L_{\text{MQW}} 2\chi_{xyz}^{(2), \text{QW}} \right) \sin\theta_r \cos\theta_r \sin 2\varphi \Big|^2, \end{aligned} \quad (8a)$$

$$\begin{aligned} \frac{I_{2\omega}^{\text{TE/TM}}}{I_\omega^2} &\propto T_{\text{TE}}^2(\theta, \omega) T_{\text{TM}}(\theta, 2\omega) A(\theta) \\ &\times \left(L_{\text{SUB}} \frac{\sin\zeta}{\zeta} e^{i\zeta} \chi_{xyz}^{(2), \text{GaAs}} \cos^2\theta_r \right. \\ &\left. + L_{\text{MQW}} \chi_{zxy}^{(2), \text{QW}} \right) \sin\theta_r \cos 2\varphi - \chi_{zxx}^{(2), \text{QW}} \sin\theta_r \Big|^2. \end{aligned} \quad (8b)$$

IV. EXPERIMENTS

In order to optically characterize our sample, we measured the fundamental conduction to valence-band transition energies in the MQW structure. The PL spectrum of the MQW structure, measured at low temperature (2 K), is plotted in Fig. 4. The sample was excited by the 482 nm line of a Kr²⁺ laser. The luminescence, dispersed with a double spectrometer, was detected by an optical multichannel analyzer. The spectrum exhibits two peaks that can be explained as follows: The main peak at 1872 meV (FWHM=14 meV) is interpreted as the recombination of

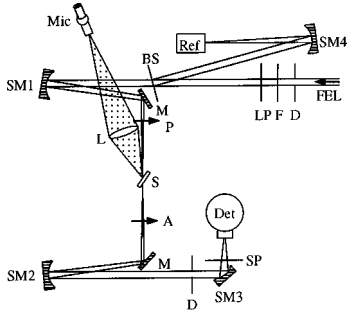


FIG. 5. Setup for the experimental SH generation experiments. FEL, free-electron laser beam; D , diaphragms; F , optical neutral density filters; LP, long-wave pass filter; BS, beam splitter; SM1–SM4, spherical and parabolic mirrors; M , planar mirrors; P , polarizer; S , sample; L , lens; Mic, microscope; A , analyzer; SP, short-wave pass filter; Det: liquid- N_2 -cooled $Hg_xCd_{1-x}Te$ detector; Ref, pyroelectric detector to reference the FEL beam intensity.

electrons confined in the first conduction miniband with holes in the first heavy-hole subband. The absence of strong phonon lines suggests that this transition is direct in space (type I), in agreement with the theoretical prediction and close to the calculated transition energy of 1852 meV. The second peak at 1825 meV is an AlAs-like LO-phonon replica of the main peak. The relatively large PL linewidth can be explained by the sensitivity of the energy of the confined states on thickness fluctuations of the 4-ML-thick GaAs layers.

Let us mention that we tried to measure the linear absorption at room temperature due to the intersubband transitions in the mid infrared with a Fourier transform spectrometer. However, the spectra were obscured by free-carrier absorption, and thus the intersubband absorption could not be observed. Further, also PL excitation measurements did not enable us to verify the energies of the higher valence subbands. These difficulties might also be due to a strongly nonparabolic in-plane dispersion of the valence subbands (see, e.g., Ref. 7) that could blur the optical transitions.

The SH generation experiments were performed at the free-electron laser user facility FELIX of the FOM Institute in Nieuwegein (Holland). The experimental setup is depicted in Fig. 5. The FEL beam was composed of macropulses with 10 μs duration and a repetition rate of 5 Hz. The macropulses themselves decompose into trains of 5 ps-wide micropulses having a repetition rate of 1 GHz. The second and third harmonics of the laser beam were first filtered out. Then the beam was split into two branches. The first branch was focused onto the sample. The other branch was focused onto a pyroelectric detector placed at the same distance from the sample to account for absorption in air. The square of its signal was then used as a reference to normalize the SH signal of the sample. The sample itself was mounted on a micropositioning stage permitting it to move in three directions and to rotate around three perpendicular axes. In this way the sample could be positioned with respect to the FEL beam as shown in Fig. 2, with the possibility to vary the inclination angle θ between 0° and 70° , and to choose φ freely with respect to the $[001]$ crystallographic axes. Using a microscope, the rotation axis z and the laser beam could be superimposed on the sample surface within about 20 μm , in

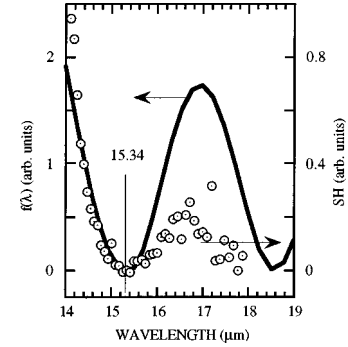


FIG. 6. SH intensity measured in the TM/TM as a function of wavelength. The dots represent data points taken at the angles $\theta = 55^\circ$ and $\varphi = 90^\circ$ on a 442 μm -thick GaAs slab. Full line, calculated phase matching factor $f(\lambda)$ [Eq. (9)].

any case the experiment was very sensitive to alignment and beam stability. The mean-power per macropulse impinging on the sample was approximately 125 mW, and the beam was focused on a spot diameter of about 100 μm ; this corresponds to a mean macropulse intensity of about 32 MW/cm² and a peak micropulse intensity of 5 GW/cm². The SH beam was separated from the transmitted (fundamental) FEL light using a filter and was focused onto a liquid- N_2 -cooled $Hg_xCd_{1-x}Te$ detector. Two wire grid polarizers were used to assure the proper polarization of the incident beam and to analyze the polarization dependence of the SH beam generated in the sample.

In order to be able to separate the MQW SH signal from the superimposed substrate contribution [cf. Eq. (7a)], the coherence length l_c and the phase mismatch ζ have to be known to a high precision.¹⁰ To calculate the coherence length [Eq. (3)], accurate values of the refractive indices n_ω , $n_{2\omega}$ are needed. Unfortunately precise data for the wavelength range between 14 and 20 μm could not be found for GaAs. The two data sets found in the literature^{12,13} do not match at 15.2 μm . As the refractive indices in the lower part of the wavelength range have been measured with a higher accuracy, we arbitrarily corrected the data of Ref. 13 by a rigid shift, in order to match the two data sets at 15.2 μm . We tested the calculated coherence length with a modified Maker fringes technique¹¹ using a blank semi-insulating GaAs substrate. The sample was kept at a fixed position, while the SH signal was acquired as a function of the exciting wavelength. At the wavelength where the phase mismatch ζ is a multiple of π , the SH signal should vanish. The result is shown in Fig. 6. The solid line represents the factor

$$f(\lambda) = \left| \frac{\sin[\zeta(\lambda)]}{\zeta(\lambda)} e^{i\zeta(\lambda)} \right|^2, \quad (9)$$

which describes the effect of the phase mismatch in Eq. (6) as a function of the wavelength λ ; it has been calculated using Eqs. (3) and (5) for a 442- μm -thick GaAs slab at an incidence angle of $\theta = 55^\circ$. The dots represent the measured SH intensity of the GaAs slab, while scanning the FEL wavelength. The measured SH signal vanishes at 15.3 μm , while the calculated one vanishes at 15.2 μm . The corresponding coherence lengths are 76.8 ± 0.2 and 76 ± 2 μm , respectively. This agreement justifies our choice of n_ω and

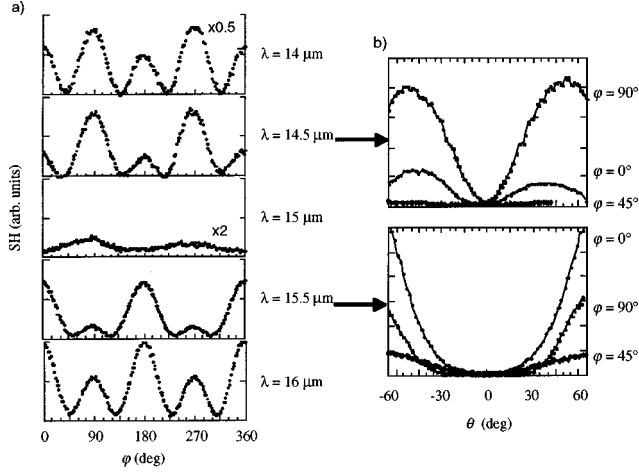


FIG. 7. Measured SH intensity in TM/TM configuration and at different wavelength, emitted by the MQW structure described in the text, (a) as a function of the angle φ , and (b) as a function of the incidence angle θ . The 180° symmetry in (a) evidences the presence of the $\chi_{zxx}^{(2)}$ and $\chi_{xxz}^{(2)}$ components of the susceptibility tensor. The angle θ in (a) is equal to 55° .

$n_{2\omega}$ in calculating the coherence length. Furthermore, the coherence length is large compared to the MQW thickness, legitimatizing the approximation made in Eqs. (7) and (8).

Examples of the measured dependence on φ and θ of the SH intensity are given in Fig. 7. Figure 7(a) shows the normalized SH intensity $I_{2\omega}/I_\omega$ as a function of the angle φ , for a fixed inclination $\theta=55^\circ$, for the TM/TM configuration, and for various wavelengths. The twofold symmetry in the φ dependence is a direct evidence for the effect of the MQW, the rotation axis being in the [001] crystallographic direction, and the structure having the low C_{2v} symmetry. On the other hand, the SH signal emitted by the cubic GaAs substrate features a fourfold symmetry in φ [as can be seen by the two terms in Eqs. (7) and (8)]. This higher symmetry has actually been observed on a sample where the MQW structure was removed, verifying the proper alignment of the experimental setup. At the wavelength of $15.3 \mu\text{m}$, the phase mismatch ζ vanishes (Fig. 6) and there is a change of sign in its phase; the effect of this behavior is clearly visible in Fig. 7.¹⁰

The θ dependence of the SH signal is shown in Fig. 7(b). The curves have been obtained for $\varphi=0^\circ$, 45° , and 90° . For $\varphi=45^\circ$, all measured θ scans show clearly a $\sin^2\theta\cos^4\theta$ -like dependence. We can therefore neglect the term containing $\chi_{zzz}^{(2)}$ which is obviously much weaker than the other components. The observable slight asymmetry in the θ dependence is due to a slight misalignment.

The dependence of the SH signal on the polarization configuration is plotted in Fig. 8. The curve with a twofold symmetry in φ has been measured in TM configuration, whereas the curve with the fourfold symmetry has been obtained in TM/TE configuration. The qualitative features of the observed φ dependencies, i.e., the symmetries, the relative strength of the maxima, the minima in TM/TM configuration not being zero, and the relative phase of the oscillations in configurations, are in agreement with the predictions of Eqs. (7) and (8). Finally, let us mention that the clear evidence of the C_{2v} symmetry in the SH signal is an indication that the contributions from the QW's is strong (the MQW structure is

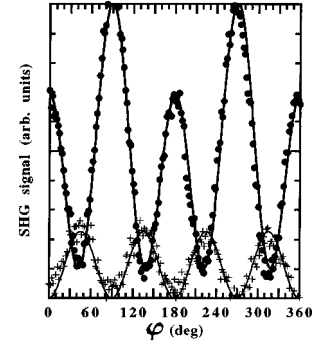


FIG. 8. SH intensity measured as a function of the angle φ in the two configurations TM/TM (dots) and TM/TE (crosses). The fundamental wavelength was $16 \mu\text{m}$ and the angle $\theta=55^\circ$. The symmetry in φ , the relative strength of the maxima, the offset of the minima in TM/TM configuration, and the phase shift between both configurations are in agreement with the theoretical expectations [the curves are fits to Eqs. (6) and (8a)].

much thinner than the coherence length) and hence that the experiments were done at frequencies close to those of the valence intersubband transitions.

V. DISCUSSION

The second-order susceptibility of the GaAs substrate can generally be taken as constant at wavelengths far from resonances.⁶ We did not find any literature values in the wavelength range from 14 to $17 \mu\text{m}$. The closest measured value has been obtained at $10.6 \mu\text{m}$.¹⁴ However, we expect the second-order susceptibility of GaAs to be affected when approaching the two-LO-phonon resonance at $19 \mu\text{m}$ (65 meV). By dividing Eq. (7a) by $3\chi_{xyz}^{(2),\text{GaAs}}$ we get an expression for the relative enhancement of the susceptibility components. Further, as mentioned above, the $\chi_{zzz}^{(2),\text{QW}}$ component is expected to be smaller than the other ones, and in addition the internal angle θ_r of the refracted FEL beam is always smaller than 17° ($\tan^2\theta_r \leq 0.07$); therefore we can neglect the term containing $\chi_{zzz}^{(2),\text{QW}}$ in Eq. (7a). We get for the normalized SH intensity

$$\begin{aligned} \frac{I_{2\omega}^{\text{TM/TM}}}{I_\omega^2} &\propto T_{\text{TM}}^2(\theta, \omega) T_{\text{TM}}(\theta, 2\omega) A(\theta) \\ &\times \left(L_{\text{SUB}} \frac{\sin\zeta}{\zeta} e^{i\zeta} + L_{\text{MQW}} \eta_{xyz} e^{i\sigma_{xyz}} \right) \cos 2\varphi \\ &+ L_{\text{MQW}} \eta_{xxz} e^{i\sigma_{xxz}} \left| \sin^2\theta_r \cos^4\theta_r \right|^2 \end{aligned} \quad (10)$$

with

$$\eta_{ijk} e^{i\sigma_{ijk}} \equiv \frac{(2\chi_{ijk}^{(2),\text{QW}} + \chi_{kij}^{(2),\text{QW}})}{3\chi_{xyz}^{(2),\text{GaAs}}}. \quad (11)$$

The real quantities η_{ijk} stand for the enhancement of the second-order susceptibility of the MQW compared to the substrate, and the phases σ_{ijk} for their relative phases.

The values of η_{xyz} , σ_{xyz} , η_{xxz} , and σ_{xxz} were considered to be parameters and have been obtained through a fit of Eq. (10) to the experimental values. The least-squares fit has

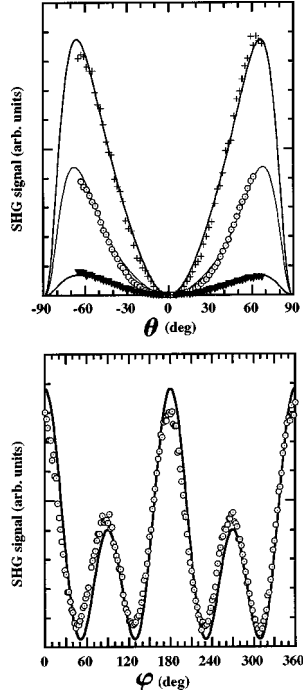


FIG. 9. Measured (dots) and fitted (lines) SH signal for TM/TM, emitted by a $462 \mu\text{m}$ -thick sample of a $4(\text{GaAs})\text{-}14(\text{Al}_{0.5}\text{Ga}_{0.5}\text{As})\text{-}12(\text{AlAs})$ MQW structure grown on a GaAs substrate. The wavelength of the exciting FEL light was kept at $16 \mu\text{m}$. The fits have been obtained using Eq. (10). The lower part shows the φ dependence for $\theta = 55^\circ$, the upper part shows the θ dependence for $\varphi = 0^\circ$ (crosses), $\varphi = 45^\circ$ (triangles) and $\varphi = 90^\circ$ (circles).

been performed using the Levenberg-Marquardt method.¹⁵ Figure 9 shows examples of the fitted angular dependence of the SH intensity at a wavelength of $16 \mu\text{m}$. The errors in the fitting are essentially due to errors in the alignment. Again it can be seen that neglecting the η_{zzz} related term in Eq. (7a) is justified by the θ dependence of the SH signal for $\varphi = 45^\circ$, since the experimental data are well modeled by Eq. (10). The wavelength dependence of the fitting parameters η and σ are summarized in Fig. 10. We think that the poor agreement between experiment and theory for η_{xyz} and σ_{xyz} is due to the fact that in the experiment the contribution to the SH signal generated by the $\chi_{xyz}^{(2),\text{QW}}$ element of the QW's is difficult to distinguish from that generated by the $\chi_{zxy}^{(2),\text{GaAs}}$ element of the substrate.

In a system with three equally spaced energy levels the double resonance for $\chi^{(2)}$ can be simplified to⁴

$$\chi^{(2)}(\omega) \propto \frac{\mu_{12}\mu_{23}\mu_{31}}{(\hbar\omega - \hbar\Omega - i\Gamma_{12})(2\hbar\omega - 2\hbar\Omega - i\Gamma_{13})}, \quad (12)$$

where $\hbar\Omega$ is the energy difference between neighboring levels involved in the transition, Γ_{ij} is the damping of the transitions, and the second-order susceptibility is proportional to the product of the three dipole-matrix elements μ_{ij} . At resonance it depends ‘‘quadratically’’ on the damping constants Γ_{ij} that depend mainly on the sample quality. The theoretical predictions shown in Fig. 3 [which have been calculated using a more general model than the three-level model of Eq.

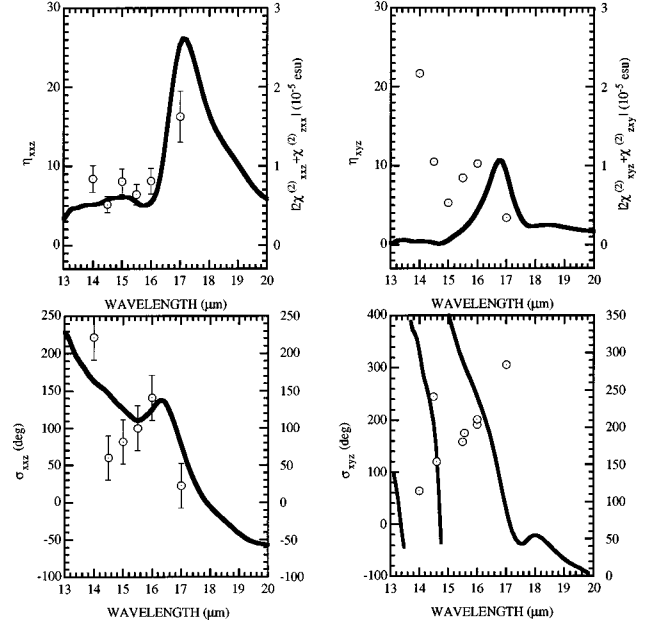


FIG. 10. Calculated and measured nonlinear susceptibility of the MQW structure described in the text. The fitted enhancement factors η_{xxz} and η_{xyz} as well as the phases σ_{xxz} and σ_{xyz} (dots) are compared to the calculated values of $(2\chi_{xxz}^{(2),\text{QW}} + \chi_{zxx}^{(2),\text{QW}})$ and $(2\chi_{xyz}^{(2),\text{QW}} + \chi_{zxy}^{(2),\text{QW}})$ (solid curves).

[12]) have been obtained assuming all damping constants equal to 3 meV. The maximum value for the sum of the susceptibility components $(2\chi_{xxz}^{(2),\text{QW}} + \chi_{zxx}^{(2),\text{QW}})$ was predicted to be 2.5×10^{-5} esu, and to occur at 0.073 eV. Compared to $3\chi_{xyz}^{(2),\text{GaAs}} = 4.5 \times 10^{-8}$ esu (at $\lambda = 10.6 \mu\text{m}$) of GaAs,¹⁴ this corresponds to an enhancement factor η of 560. This predicted enhancement for our valence-band structure is about a factor of 48 weaker than the ones measured in samples using conduction intersubband transitions,⁵ differences in the damping constants have been accounted for. The main reasons for this difference lie in the warping of the bulk HH valence band and the coupling between HH and LH occurring in the QW's. These effects, which are absent in conduction subbands, result in the reduction of the intersubband density of states and affect the enhancement as mentioned above. This disadvantage is partly compensated by the absence of the small factor $\tan^2\theta$, (≤ 0.07) for the non- $\chi_{zzz}^{(2)}$ -like susceptibility components, leading to a second-harmonic efficiency of the valence intersubband transitions that is only about 3.4 times lower than that of the conduction subbands. Further, larger damping constants result in a broadening of the resonances and reduced magnitudes of $\chi^{(2)}$.⁷ Our sample has considerably larger linewidths than the above-mentioned 3 meV, as can be seen from the PL spectrum in Fig. 4. If we correct the predicted magnitude for a damping constant of 14 meV (PL linewidth, lower limit) we would [according to Eq. (12)] expect an enhancement of not more than 25. The enhancement of 16 we deduce from our SH measurements lies close to this value and is about twice the enhancement measured in single resonant valence-band structures.^{7,8}

VI. CONCLUSIONS

We demonstrated SH generation in p -doped $\text{GaAs}/\text{Al}_x\text{Ga}_{1-x}\text{As}$ asymmetrically stepped MQW structures.

The experiments were done with the light emitted by a FEL close to $16 \mu\text{m}$, exploiting the enhancement of the second-order susceptibility when the energy of the incoming photons is close to that of the transitions between the first heavy-hole, first light-hole, and second heavy-hole subbands. We measured the directional, wavelength, and polarization dependence of the SH signal. The presence of the $\chi_{xyz}^{(2),\text{QW}}$, $\chi_{zxy}^{(2),\text{QW}}$ and $\chi_{xzx}^{(2),\text{QW}}$, $\chi_{zxx}^{(2),\text{QW}}$ elements in the second-order susceptibility tensor has been verified, in agreement with theoretical predictions. This contrasts with SH generation experiments involving conduction subbands where the $\chi_{zzz}^{(2),\text{QW}}$ element is dominant. The measured maximum enhancement of 16 of the second-order susceptibility of the QW's with respect to that of bulk GaAs agrees with the theoretical expectations with the quality of the investigated samples taken into account. Possible devices making use of valence intersubband transitions, compared to those using conduction inter-

subband transitions, benefit from the possibility to work with TE polarized input fields that are easy to transmit into the MQW structure, and from the possibility to generate SH output having a polarization which is different from that of the input wave.

ACKNOWLEDGMENTS

We gratefully acknowledge the support by the Stichting voor Fundamenteel Onderzoek der Materie (FOM) in providing the required beam time on FELIX and highly appreciate the skillful assistance by the FELIX staff. We would like to thank E. Martinet at EPF Lausanne for useful discussions. This work has been supported in part by the Fonds National Suisse de la Recherche Scientifique. M.J.S. would like to acknowledge the support by the U.S. Office of Naval Research.

-
- ¹J. S. Harris, Jr. and M. M. Fejer, Proc. SPIE **1361**, 262 (1991).
²P. Boucaud, F. H. Julien, D. D. Yang, J.-M. Lourtioz, R. E. P. Bois, and J. Nagle, Appl. Phys. Lett. **57**, 215 (1990).
³H. C. Chui, E. L. Martinet, G. L. Woods, M. M. Fejer, J. S. Harris, Jr., C. A. Rella, B. I. Richman, and H. A. Schwetman, Appl. Phys. Lett. **64**, 3365 (1994).
⁴J.-Y. Duboz, P. Bois, and E. Rosencher, in *Confined Electrons and Photons*, edited by E. Burstein and C. Weissbuch (Plenum, New York, 1995).
⁵E. L. Martinet, G. L. Woods, H. C. Chui, J. S. Harris, Jr., M. M. Fejer, C. A. Rella, and B. A. Richman, Proc. SPIE **2139**, 331 (1994).
⁶P. N. Butcher and D. Cotter, *The Elements of Nonlinear Optics* (Cambridge University Press, Cambridge, 1993).
⁷M. J. Shaw, M. Jaros, Z. Xu, P. M. Fauchet, C. W. Rella, B. A. Richman, H. A. Schwetman, and G. W. Wicks, Phys. Rev. B **50**, 18 395 (1994).
⁸Z. Xu, P. M. Fauchet, C. W. Rella, B. A. Richman, H. A. Schwetman, and G. W. Wicks, Solid State Commun. **93**, 903 (1995).
⁹G. Bastard, *Wave Mechanics Applied to Semiconductor Heterostructures* (Les Éditions de Physique, Les Ulis Cedex, France, 1992).
¹⁰E. L. Martinet, H. C. Chui, G. L. Woods, M. M. Fejer, and J. S. Harris, Jr., Appl. Phys. Lett. **65**, 1 (1994).
¹¹Y. R. Shen, *The Principles of Nonlinear Optics* (Wiley, New York, 1984).
¹²A. N. Pikhtin and A. D. Yas'kov, Fiz. Tekh. Poluprovodn. **12**, L047 (1978) [Sov. Phys. Semicond. **12**, 622 (1978)].
¹³W. Cochran, S. J. Fray, F. A. Quarrington, and W. Williams, J. Appl. Phys. Suppl. **34**, 2102 (1961).
¹⁴B. F. Levine and C. G. Bethea, Appl. Phys. Lett. **20**, 272 (1972).
¹⁵W. H. Press *et al.*, *Numerical Recipes* (Cambridge University Press, Cambridge, 1986).